



Contents lists available at ScienceDirect

Journal of King Saud University – Science

journal homepage: www.sciencedirect.com

Original article

Investigation of structural and electrical properties of synthesized Sr-doped lanthanum cobaltite ($\text{La}_{1-x}\text{Sr}_x\text{CoO}_3$) perovskite oxide

Norah Alhokbany^{a,*}, Sultanah Almotairi^a, Jahangeer Ahmed^{a,*}, Sameerah I. Al-Saeedi^b, Tansir Ahamad^a, Saad M. Alshehri^{a,*}^a Department of Chemistry, College of Science, King Saud University, Riyadh 11451, Saudi Arabia^b Department of Chemistry, College of Science, Princess Nourah Bint Abdulrahman University, Riyadh, Saudi Arabia

ARTICLE INFO

Article history:

Received 3 March 2021

Revised 21 March 2021

Accepted 22 March 2021

Available online 27 March 2021

Keywords:

 $\text{La}_{1-x}\text{Sr}_x\text{CoO}_3$

Perovskites

X-ray

Crystal structure

Dielectric

ABSTRACT

Sr-doped lanthanum cobaltite ($\text{La}_{1-x}\text{Sr}_x\text{CoO}_3$) perovskite oxides with $x = 0.0, 0.20, 0.50, 0.80$ were prepared using the modified sol-gel method at 600 °C. The synthesized Sr-doped LaCoO_3 perovskite oxides ($x = 0.0$ and 0.20) crystallize as rhombohedral structured materials, while $\text{La}_{0.2}\text{Sr}_{0.8}\text{CoO}_3$ perovskite oxide ($x = 0.80$) crystallizes as primitive cubic structured material as also confirmed by Rietveld refinement using x-ray diffraction. Moreover, the synthesized materials were investigated in details using fourier-transform infrared spectroscopy, scanning electron microscopy, energy dispersive studies and x-ray photoelectron spectroscopy techniques. The electrical conductivity of the perovskite oxides was improved through the substitution of La by Sr. Frequency dependent dielectric properties (dielectric constant and dielectric loss) of $\text{La}_{1-x}\text{Sr}_x\text{CoO}_3$ perovskite oxides were also investigated in frequency range from 20 Hz to 3 MHz at room temperature. Dielectric constant and dielectric loss of $\text{La}_{1-x}\text{Sr}_x\text{CoO}_3$ perovskite oxides decrease at low frequency, while it was found to be constant at high frequency.

© 2021 The Authors. Published by Elsevier B.V. on behalf of King Saud University. This is an open access article under the CC BY-NC-ND license (<http://creativecommons.org/licenses/by-nc-nd/4.0/>).

1. Introduction

ABO_3 type LaCoO_3 (lanthanum cobaltite) perovskite oxides have two different sized cations of A-site with rare earth element and B-site with transition element surrounded by oxygen anions show great interest in diverse applications including optical (Farhadi and Sepahvand 2010), magnetic (Bellakki et al., 2010), thermoelectric (Kun et al., 2013), electro-catalysis (Jayapandi et al., 2018; Lu et al., 2019), photo-catalysis (Fu et al., 2013; Jayapandi et al., 2018), fuel cells (Rehman et al., 2018) and sensing (Wang et al., 2017) applications. LaCoO_3 perovskite oxides also exhibit good conductivity (Huang et al., 1998; Nakayama et al., 2003; Zhu et al., 2018). Thermally stable LaCoO_3 perovskite oxides have stable crystal structure and can be used as electrode material for high-

temperature solid oxide fuel cells (SOFCs) (Rehman et al., 2018). Physico-chemical and catalytic properties of ABO_3 perovskites can be influenced efficiently with the substitution of A-site by other elements. The oxygen vacancy defects in perovskite also play an important role in the mobility of oxygen from the crystalline oxygen to the surface oxygen of perovskite. Sr-doped LaCoO_3 perovskite oxides (i.e. $\text{La}_{1-x}\text{Sr}_x\text{CoO}_3$) are recently reported as excellent bifunctional electro-catalysts in oxygen reduction and oxygen evolution reactions (ORR/OER) due to high surface area, virtuous electronic conductivity and unique electronic structure (Cheng et al., 2015; Mefford et al., 2016). $\text{La}_{1-x}\text{Sr}_x\text{CoO}_{3-\delta}$ perovskite oxides have also shown interesting crystal structure, magnetic behaviour, thermal and electrical properties (Iwasaki et al., 2008; Petrov et al., 1995). Thermal studies and crystal structure of nickel-substituted $\text{La}_{0.5}\text{Sr}_{0.5}\text{CoO}_{3-\delta}$ ceramics have been reported with enhanced electrical properties (Lu et al., 2020). Sr or Ce doped LaCoO_3 perovskites could be promising materials due to electronic configuration and electrical conductivity as also reported elsewhere (Hwang et al., 2017; Wang et al., 2010). $\text{La}_{1-x}\text{Sr}_x\text{CoO}_3$ perovskite oxides have been used extensively as magnetic (Chennabasappa et al., 2020), thermoelectric (Viskadorakis et al., 2019), optical (Fang et al., 2016) and electro-catalytic (Lal et al., 2005) materials for various applications. Magneto-caloric effect (Long et al., 2018) and structural properties (Li et al., 2019) of $\text{La}_{1-x}\text{Sr}_x\text{CoO}_3$ perovskite oxides

* Corresponding authors.

E-mail addresses: nhokbany@ksu.edu.sa (N. Alhokbany), jahmed@ksu.edu.sa (J. Ahmed), alshehri@ksu.edu.sa (S.M. Alshehri).

Peer review under responsibility of King Saud University.



Production and hosting by Elsevier

<https://doi.org/10.1016/j.jksus.2021.101419>

1018-3647/© 2021 The Authors. Published by Elsevier B.V. on behalf of King Saud University.

This is an open access article under the CC BY-NC-ND license (<http://creativecommons.org/licenses/by-nc-nd/4.0/>).

were also reported for oxygen storage application. $\text{La}_{1-x}\text{Sr}_x\text{CoO}_3$ perovskite oxides were also reported as good electrical conducting materials and used as cathode materials in SOFCs (Björketun et al., 2017; Wu et al., 2017). The electrical conductivity and the crystal structure of $\text{La}_{1-x}\text{Sr}_x\text{CoO}_3$ depend on Sr-doping and temperature (Wu et al., 2017). Electrical and thermal properties could be affected by the structural change of $\text{La}_{1-x}\text{Sr}_x\text{CoO}_3$ perovskite oxides (Liu et al., 2016; Viskadourakis et al., 2016). $\text{La}_{1-x}\text{Sr}_x\text{CoO}_3$ perovskite materials were also used as sensor for acetone sensing at room temperature (Liu et al., 2017). An attractive and promising way has also been designed for white and green light emitting phosphorus materials (Khan et al., 2018, 2017). Recently, we have developed $\text{La}_2\text{MnNiO}_6$ (Ahmed et al., 2020), $\text{Na}_2\text{La}_2\text{P}_4\text{O}_{12}$ (Alhokbany et al., 2020) and $\text{NiMoO}_4@\text{rGO}$ (Ahmed et al., 2021) electrode materials for energy conversion and energy storage applications. Herein, we report synthesis of $\text{La}_{1-x}\text{Sr}_x\text{CoO}_3$ perovskite oxides at different compositions ($x = 0.0, 0.20, 0.50, 0.80$) using the sol-gel method at 600 °C. Structural and electrical prop-

erties of $\text{La}_{1-x}\text{Sr}_x\text{CoO}_3$ perovskite oxides were successfully investigated in details.

2. Experimental

$\text{La}_{1-x}\text{Sr}_x\text{CoO}_3$ perovskite oxides by varying the compositions were prepared using the modified sol-gel method (Ahmed et al., 2016). The starting reagents such as $\text{La}(\text{NO}_3)_3 \cdot 6\text{H}_2\text{O}$ (Sigma Aldrich, 99%), $\text{Co}(\text{NO}_3)_2 \cdot 6\text{H}_2\text{O}$ (Sigma Aldrich, 98%) and $\text{Sr}(\text{NO}_3)_2$ (Sigma Aldrich, 99.9%) were taken in an appropriate stoichiometric ratio with excess of citric acid (Sigma Aldrich, 99%) and transferred to the porcelain crucible containing de-ionized water followed by the formation of viscous gel. The evaporation of water was taken place for dryness and then calcined the materials at 400 °C/2h and 600 °C/10 h at constant heating rate of 10C/min. $\text{La}_{1-x}\text{Sr}_x\text{CoO}_3$ perovskite oxides ($x = 0.0, 0.20, 0.50, 0.80$) were obtained using the above process at 600 °C. The proposed reaction in the synthesis of $\text{La}_{1-x}\text{Sr}_x\text{CoO}_3$ perovskite oxides is given as:

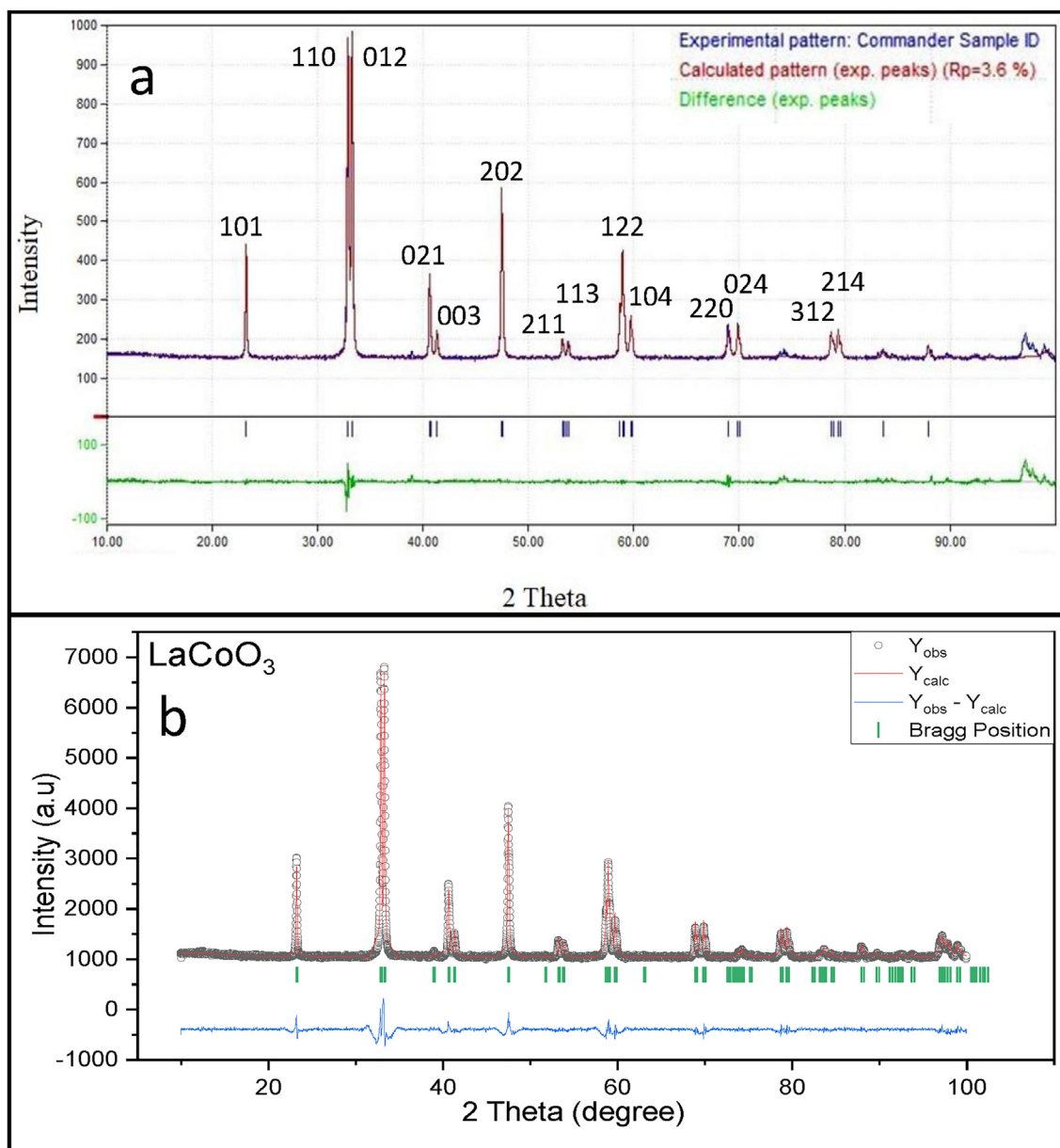


Fig. 1. (a) X-ray diffraction patterns and (b) Rietveld refinement of LaCoO_3 perovskite oxide.

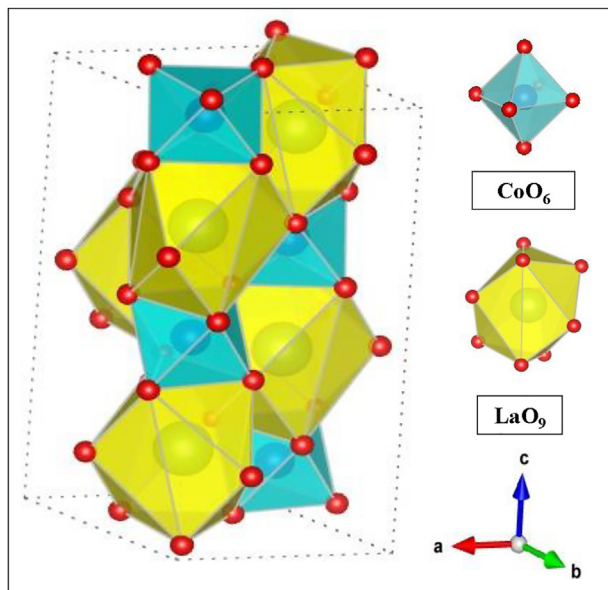
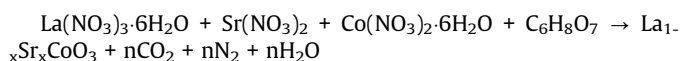


Fig. 2. Crystal structure of rhombohedral unit cell of LaCoO₃ perovskite oxide.



The synthesized La_{1-x}Sr_xCoO₃ perovskite oxides were characterized using powder x-ray diffraction (XRD) followed by Rietveld refinement using the fullprof program (Reis et al., 2017; Rodríguez-Carvajal, 1993). XRD data was recorded on Bruker D-8 Advance diffractometer in 2θ range between 10 and 100° at the rate of 0.01°/second. XRD diffractometer contains Ni filtered CuKα radiation. The cell parameters were refinement by fullprof software, match software (personal licenses- version 3.6.2.121- Crystal Impact, Bonn, Germany) based on the Rietveld refinement method. Match software was used to carry out search and match technique with an international database i.e. crystallography open database (COD) to identify the unknown phases. The peak position and relative intensities of the experimental (observe) data and reference

(calculate) data were used in fitting to obtain the best matching between them. Fourier-transform infrared spectroscopy (FTIR) data was collected on Bruker TENSOR 27 Spectrometer. The samples for FTIR measurements were prepared with KBR followed by the palletization at room temperature. Scanning electron microscopic (SEM) studies of La_{1-x}Sr_xCoO₃ perovskite oxides were carried out with JEOL JSM-7600F machine for surface morphology. The oxidation states of the elements were investigated by x-ray photoelectron spectroscopy (XPS) using a Thermo Scientific Theta Probe Angle-Resolved XPS system (USA). Details of the calibration of XPS were reported elsewhere (Dobler et al., 2002). The instrument was run with a standard Al-Kα source radiation with the photon energy of 1486.6 eV and operated at 9 kV and 20 mA. Pass energy values of 200 eV and 50 eV were employed for survey scans and detailed scans, respectively. The data were corrected for any drift by setting the binding energies were referenced to C1s peak at 284.8 eV. The electrical conductivity and dielectric measurements were recorded with Wayne Kerr 6440B Precision Component Analyzer at different frequency range from 20 Hz to 3 MHz.

3. Results and discussion

The lattice parameters of the prepared materials are resulted from the fitting of the experimental diffraction patterns by Rietveld refinement. The powder XRD patterns of LaCoO₃ are shown in Fig. 1a. Rietveld refinement method displays smaller values of R_{wp} (i.e. 22.2%) and R_p, which imply the best fit as shown in Fig. 1b. The resulting fitting patterns confirm the formation of pure phase material. The XRD patterns of LaCoO₃ show single-phase and could be indexed with rhombohedral (space group of R-3c), and consistent with standard JCPDS file # 04-013-6817 (Haron et al., 2017). These results are also in good agreement with previous reports (Cheng et al., 2015; Haron et al., 2017). Major diffraction peaks were detected at two theta (2θ) of 23.25°, 32.89°, 33.27°, 40.73°, 41.38°, 47.48°, 53.36°, 53.78°, 58.93°, 59.71°, 68.97°, 70.04° 78.74°, and 79.42° correspond to the lattice planes such as (101), (110), (012), (021), (003), (202), (211), (113), (122), (104), (220), (024), (312) and (214) respectively, which detected the high degree of La and Co incorporated in the perovskite lattice structure. The characteristic doublet highest intensity peaks at (20)

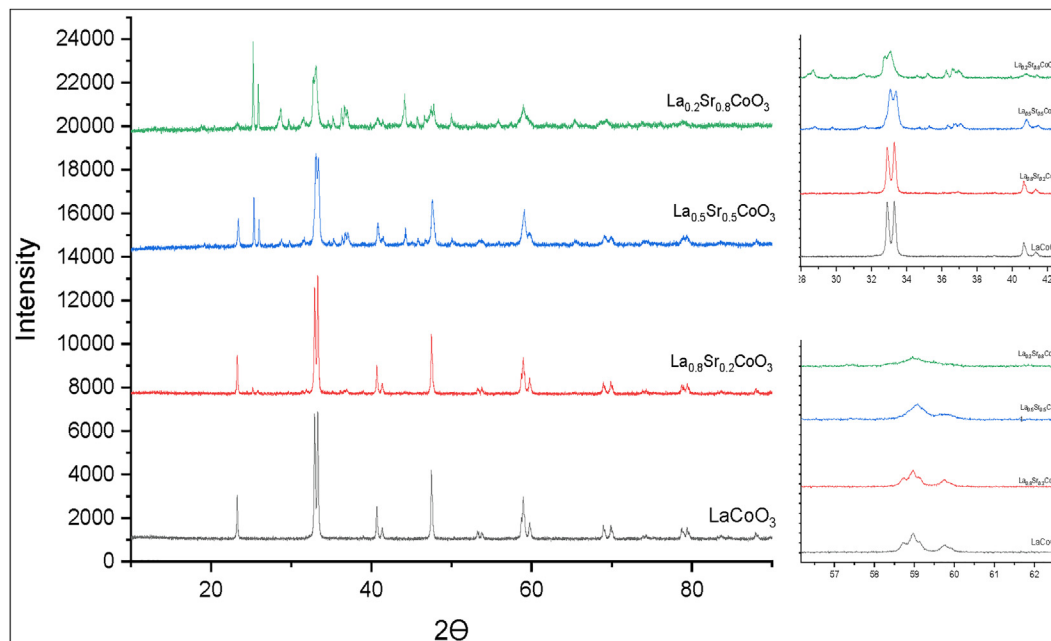


Fig. 3. XRD patterns of La_{1-x}Sr_xCoO₃ perovskite oxides showing shift to higher 2θ degrees for samples with Sr compared with un-doped LaCoO₃.

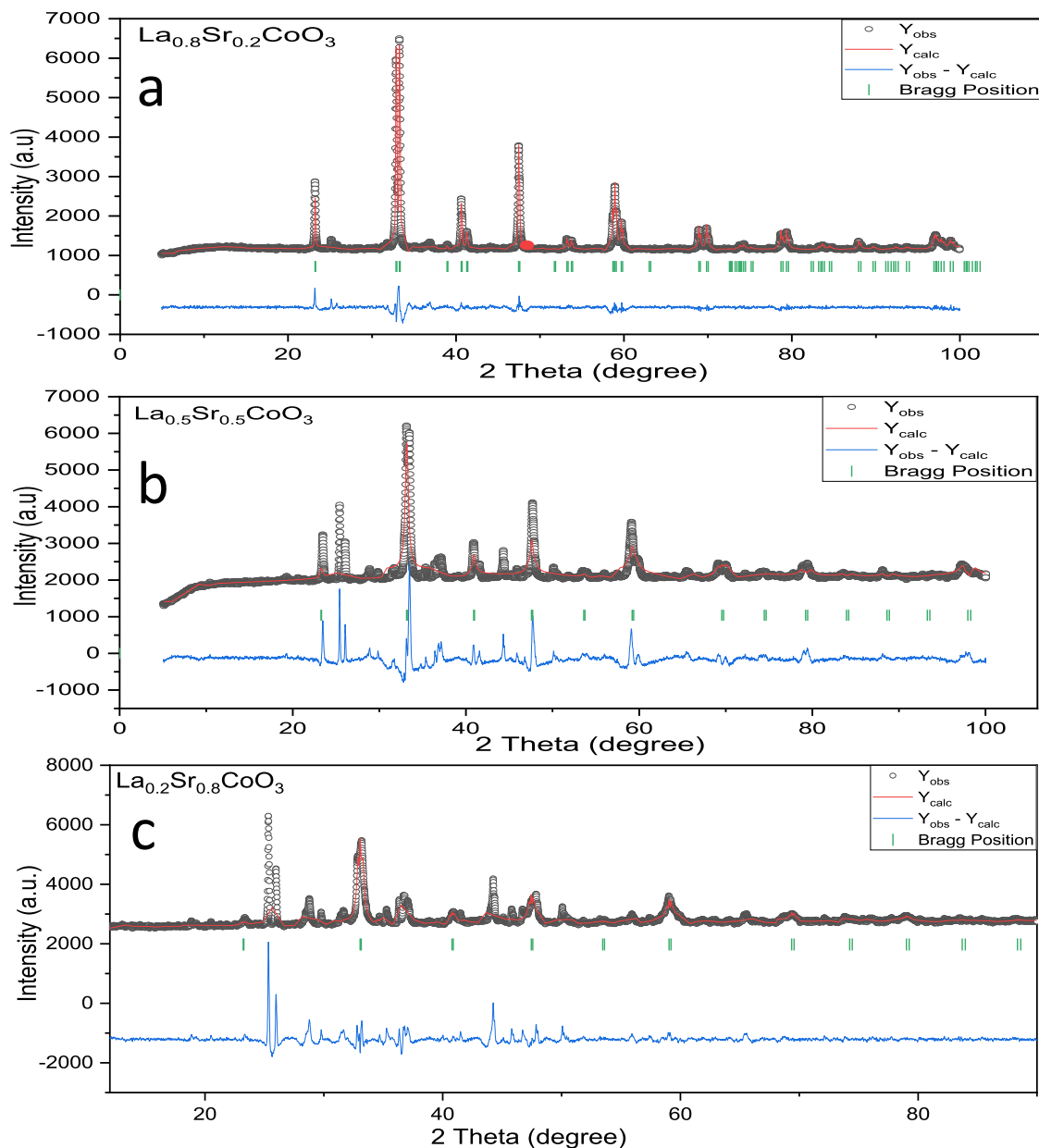


Fig. 4. Rietveld refinement of $\text{La}_{1-x}\text{Sr}_x\text{CoO}_3$ perovskite oxides ($x = 0.20, 0.50, 0.80$).

of 32.89° and 33.27° indicate that the calcination temperature had a significant effect on the formation of the perovskite phase. The sharp diffraction peaks of LaCoO_3 reveal its high crystalline nature with no impurities such as La_2O_3 and Co_3O_4 phase. Rietveld refinement of XRD patterns shows good profile fitting patterns of experimental and calculated profile data, which can be identified with rhombohedral symmetry (space group of R-3c). The refined unit cell parameters of rhombohedral structure were found to be “a”= 5.4461 Å, “b”= 5.4461 Å, “c”= 13.1077 Å, “ α ”=90.000°, “ β ”=90.06 4° and “ γ ”=180.000°. Fig. 2 shows the crystal structure of the unit cell of LaCoO_3 along with a-axis. In this structure, Co^{3+} and La^{3+} cations are 6-fold and 9-fold coordinated with oxygen anion, respectively. This trigonal symmetry involves an alternating rotation of the octahedral CoO_6 subunits connected through corner-shared oxygen. In the axes sittings, the structure has been described by the lattice constants of rhombohedral angle (α) and oxygen coordinated (x). The oxygen atoms are fully occupied 18e

(x,0,1/4) sites in the unit cell of LaCoO_3 . Fig. 3 shows the XRD patterns of the $\text{La}_{1-x}\text{Sr}_x\text{CoO}_3$ ($x = 0.0, 0.20, 0.50, 0.80$). From the XRD studies, we observed clearly a phase transition from the rhombohedral structure (space group of R-3c) of $\text{La}_{1-x}\text{Sr}_x\text{CoO}_3$ ($x = 0.0, 0.20$) to the cubic structure (space group of Pm-3 m) of $\text{La}_{1-x}\text{Sr}_x\text{CoO}_3$ ($x = 0.50, 0.80$). We have observed that the diffraction angle of the prepared materials gradually shifted toward small diffraction angles with increasing Sr^{2+} contents in perovskite unit cell. This can be ascribed to the successive replacement of smaller La^{3+} cation ($r_{\text{La}^{3+}}=0.136$ nm) by bigger Sr^{2+} cation ($r_{\text{Sr}^{2+}}=0.144$ nm), leading to the expansion of perovskite unit cell. Due to the high tolerance of the perovskite structure to distortion with metallic elements of different sizes and oxidation states, substitution of La^{3+} with a higher ionic radius of Sr^{2+} into the A site of LaCoO_3 maintained the rhombohedral structure at low strontium substitution levels ($x \leq 0.50$) with doublet peak at 2θ of $33\text{--}34^\circ$. By increasing the strontium substitution (i.e. $x = 0.80$), the doublet

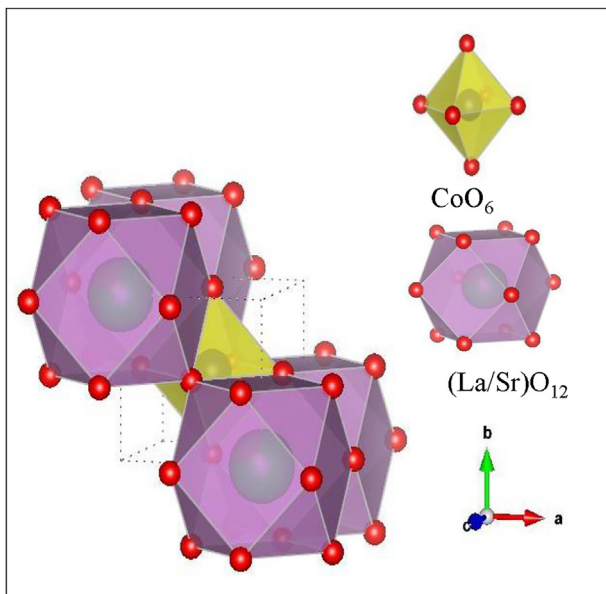


Fig. 5. Crystal structure of the cubic unit cell of $\text{La}_{0.2}\text{Sr}_{0.8}\text{CoO}_3$ perovskite oxide.

peak suggested that rhombohedral structure became weaker and slowly changed to singlet peak which indicates the formation of cubic symmetry. This is noteworthy that the crystal symmetry changes from rhombohedral to cubic at higher strontium substitution ($x = 0.80$) due to different ionic radii between La^{3+} and Sr^{2+} and the diffraction lines of $\text{La}_{1-x}\text{Sr}_x\text{CoO}_3$ gradually shifted to lower 2θ side.

Fig. 4 shows Rietveld refinement of XRD patterns of $\text{La}_{1-x}\text{Sr}_x\text{CoO}_3$ perovskite oxides ($x = 0.20, 0.50, 0.80$). Fig. 5 shows the pro-

jection of the cubic crystal structure of $\text{La}_{0.2}\text{Sr}_{0.8}\text{CoO}_3$ perovskite oxide along with 'ac' plane. The basic units of the composites are $(\text{La}/\text{Sr})\text{-O}_{12}$ and CoO_6 octahedral. The $(\text{La}/\text{Sr})\text{-O}_{12}$ sharing oxygen atoms with the CoO_6 by corner-sharing and La/Sr atoms are fully occupied in the Wyckoff position 1a. An interatomic distance of La/Sr-O bond shows bond length of 2.76 Å. In CoO_6 octahedral, Co atoms are locating in Wyckoff position 1b at the position of (0.5,0.5,0.5). Each CoO_6 shows the bond length of the Co-O bond is of 1.90 Å with bond angle Co-O-Co of 180° . This is noteworthy that present XRD studies of $\text{La}_{1-x}\text{Sr}_x\text{CoO}_3$ perovskite oxides are in good agreement with previous reports (Cheng et al., 2015; Mefford et al., 2016). Table 1 present the refinement agreement factors, cell parameters, atomic coordination, and selected inter-atomic distance. According to XRD results, the substitution of La^{3+} by the larger Sr^{2+} cations aligned the Co-O-Co atoms (from 161.6° of LaCoO_3 to ideal 180° of $\text{La}_{0.2}\text{Sr}_{0.8}\text{CoO}_3$), resulting in a structural change from a rhombohedral perovskite to a cubic structure. The unit cell also decreased and mainly attributed to the transition of Co^{3+} , with an ionic radius of (0.61 Å) to the smaller ion Co^{4+} (0.53 Å).

Electron microscopic studies of $\text{La}_{1-x}\text{Sr}_x\text{CoO}_3$ ($x = 0.0, 0.20, 0.50, 0.80$) perovskite oxides were also conducted for surface morphology and particles size analysis. SEM studies of $\text{La}_{1-x}\text{Sr}_x\text{CoO}_3$ perovskite oxides reveal the formation of uniformed particles in the particle size range from 100 to 150 nm as also seen in Fig. 6 (a-c). This is clearly visible that the average particle size increases with substitution Sr^{2+} cations for La^{3+} cations. Therefore, sub-micron sized particles of $\text{La}_{1-x}\text{Sr}_x\text{CoO}_3$ ($x = 0.80$) were detected with high concentration of Sr^{2+} (Fig. 6d). Elemental studies of $\text{La}_{1-x}\text{Sr}_x\text{CoO}_3$ perovskite oxides were carried out by energy dispersive studies (EDS) equipped with SEM. EDS data confirmed that the initial loaded compositions were matched with the resulted composition as summarized in Table 2. Fig. 7a shows FT-Infrared spectra of $\text{La}_{1-x}\text{Sr}_x\text{CoO}_3$ perovskite oxides. The O-Co-O bending

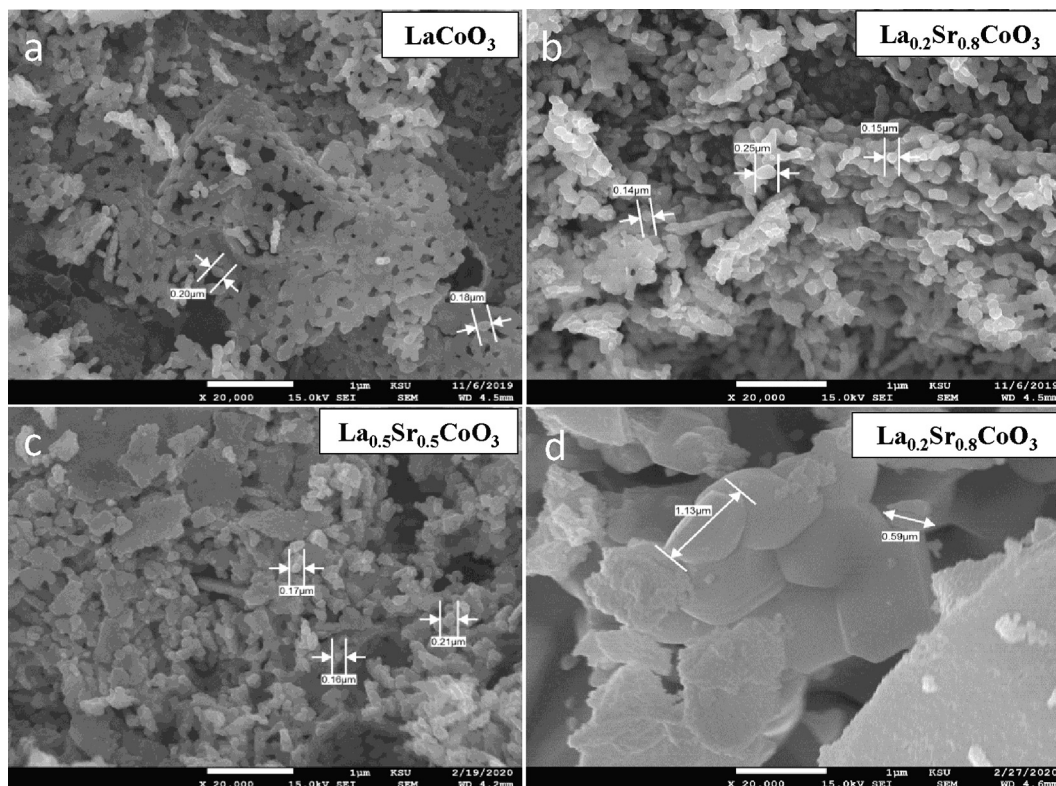


Fig. 6. SEM micrographs of $\text{La}_{1-x}\text{Sr}_x\text{CoO}_3$ perovskite oxides.

Table 1Lattice parameters and interatomic distance of the unit cell for $\text{La}_{1-x}\text{Sr}_x\text{CoO}_3$ perovskite oxides calculated from XRD patterns using Rietveld refinements.

	LaCoO_3	$\text{La}_{0.8}\text{Sr}_{0.2}\text{CoO}_3$	$\text{La}_{0.5}\text{Sr}_{0.5}\text{CoO}_3$	$\text{La}_{0.2}\text{Sr}_{0.8}\text{CoO}_3$
Space group	Rhombohedral R-3c (167)	Rhombohedral R-3c (167)	Cubic Pm-3 m (221)	Cubic Pm-3 m (221)
a (Å)	5.4461 Å	5.4458 Å	3.8200 Å	3.8288 Å
b (Å)	5.4461 Å	5.4458 Å	–	–
c (Å)	13.1077 Å	13.1103 Å	–	–
d(La/Sr-O1)	2.70 Å	2.72 Å	2.75 Å	2.76 Å
d(Co-O1)	1.93 Å	1.92 Å	1.91 Å	1.90 Å
Co-O-Co angle	161.6°	164.3°	180°	180°

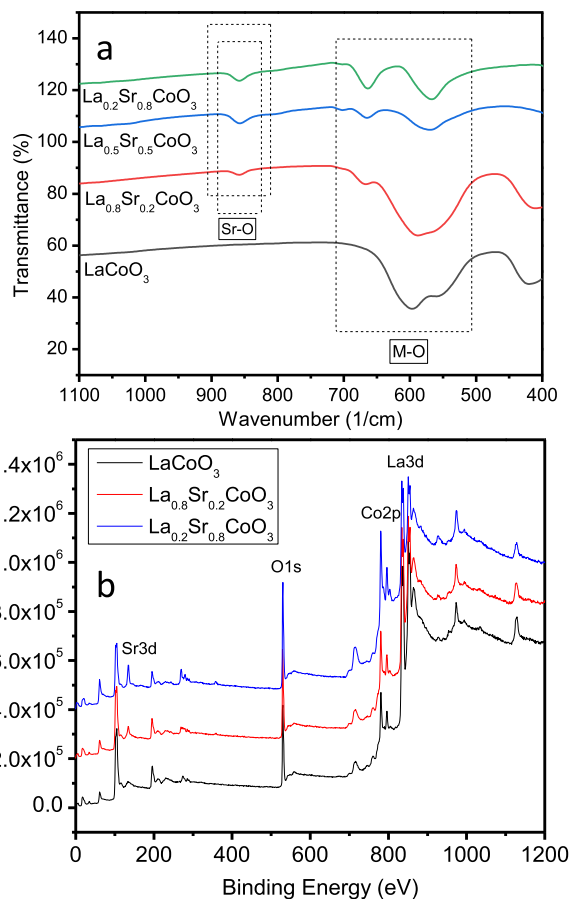
Table 2

Elemental compositions of the perovskite oxides determined from EDS studies.

Materials	Concentration (atomic %)							
	La		Sr		Co		O	
	Exp	Theo	Exp	Theo	Exp	Theo	Exp	Theo
LaCoO_3	19.42	20	–	–	17.11	20	63.47	60
$\text{La}_{0.8}\text{Sr}_{0.2}\text{CoO}_3$	14.49	16	2.69	4	16.64	20	66.19	60
$\text{La}_{0.2}\text{Sr}_{0.8}\text{CoO}_3$	4.17	4	11.85	16	20.43	20	63.55	60

and Co-O stretching vibrations of octahedral coordinated CoO_6 were detected at $\sim 420\text{ cm}^{-1}$ and $\sim 600\text{ cm}^{-1}$, respectively. The appeared band at $\sim 600\text{ cm}^{-1}$ resembles to both doped and undoped perovskite materials due to La-O vibration. FT-IR band at $\sim 852\text{ cm}^{-1}$ was attributed to Sr-O vibrations in doped samples. XPS studies of $\text{La}_{1-x}\text{Sr}_x\text{CoO}_3$ perovskites were also conducted for elemental and surface composition analysis. XPS spectra of $\text{La}_{1-x}\text{Sr}_x\text{CoO}_3$ perovskites clearly refer to La3d, Co2p, Sr3d and O1s as also shown in Fig. 7b. XPS peaks at $\sim 780\text{ eV}$ and $\sim 796\text{ eV}$ resemble to $\text{Co}2p_{3/2}$ and $\text{Co}2p_{1/2}$ respectively of Co^{3+} . A satellite peak was appeared at $\sim 786\text{ eV}$, which could be suggested a small amount of Co^{2+} on the surface of the materials. XPS peaks at ~ 834 and $\sim 854\text{ eV}$ can be associated with $\text{La}3d_{5/2}$ and $\text{La}3d_{3/2}$ respectively and existed in tri-valence state (La^{+3}). The binding energy of $\sim 134\text{ eV}$ can be referred to Sr $3d_{5/2}$ which is existed in divalence state (Sr^{+2}). After Sr^{+2} doping, the signal at $\sim 531\text{ eV}$ increases which indicates the improvement of oxygen adsorption after partial substitution of Sr^{+2} for La^{+3} . XPS peak at $\sim 528\text{ eV}$ could be associated with O1s of surface lattice oxygen ($\text{O}_{\text{latt}}^{2-}$), whereas XPS peaks at $\sim 531\text{ eV}$ can be assigned to adsorbed oxygen ($\text{O}_{\text{ads}}^{2-}$) species. It is confirmed by the surface $\text{O}_{\text{ads}}/\text{O}_{\text{latt}}$ ratio that increases from 0.77 to 1.05 after doping of Sr^{+2} to LaCoO_3 lattice.

Variation in the electrical conductivity of $\text{La}_{1-x}\text{Sr}_x\text{CoO}_3$ perovskite oxides ($x=0.0, 0.20, 0.50, 0.80$) was measured as a function of Sr doping with frequency at room temperature (Fig. 8a). Electrical conductivity relaxation has been examined using four-point DC method. The geometry of the samples was kept as rectangular with the area of $1.0\text{ cm} \times 5.0\text{ cm}$ and thickness of 1–2 mm. The following equation was used to calculate the conductivity of the perovskite oxides: $\sigma = L / R \cdot A$; where 'R' is dc resistance, 'L' is thickness of pellet, and A is cross-sectional area of the flat surface of the pellet. It was observed that the values of electrical conductivity (σ) increasing with increase in the Sr content at La site. Electrical conductivity (σ) was increased four orders of magnitude as the Sr concentration increased. LaCoO_3 perovskite oxide act as a charge-transfer insulator and doping of Sr^{2+} into La^{3+} site introduces hole carriers in $\text{La}_{1-x}\text{Sr}_x\text{CoO}_3$ perovskite oxides (Lu et al., 2020; Mineshige et al., 1996). Therefore, high electrical conductivity may be attributed to increase the hole concentration with Sr-substitution in LaCoO_3 perovskite oxide. The dielectric properties of the materials depend on the applied frequency, temperature and grain boundaries. Frequency dependent dielectric measurements of $\text{La}_{1-x}\text{Sr}_x\text{CoO}_3$ perovskite oxide materials were carried out at room temperature. Fig. 8(a) and (b) show the variation of dielectric constant and dielectric loss

**Fig. 7.** (a) FTIR spectra and (b) XPS survey of $\text{La}_{1-x}\text{Sr}_x\text{CoO}_3$ perovskite oxides.

of $\text{La}_{1-x}\text{Sr}_x\text{CoO}_3$ perovskite oxide materials as a function of frequency of applied field (20 Hz–3 MHz) at room temperature. Fig. 8b illustrates that the dielectric constant (ϵ') decreases with increasing frequency and becomes almost frequency independent at high frequency. This could be ascribed to the normal behaviour of the dielectric materials due to the relaxation behaviour of the system. Larger value of dielectric constant at lower frequency could be due to the accumulation of ions at the interface of conducting

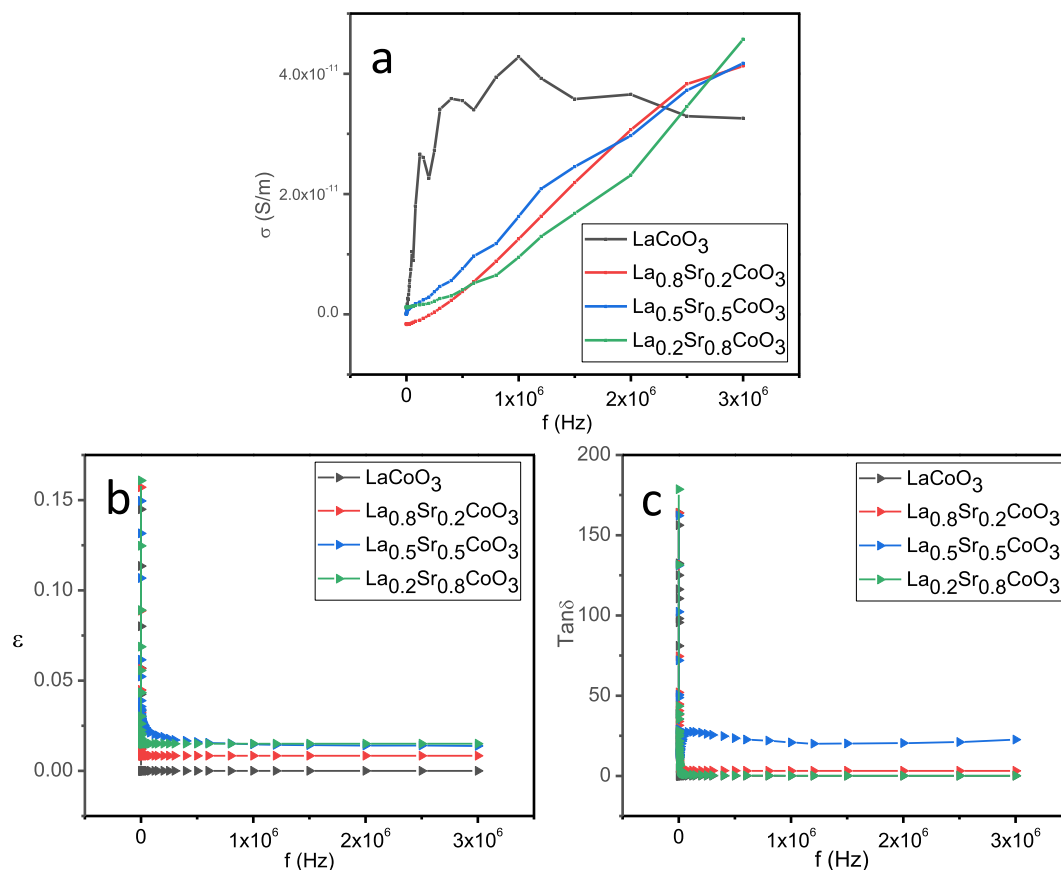


Fig. 8. (a) Variation of DC conductivity with frequency for La_{1-x}Sr_xCoO₃ perovskite oxides. (b) Plot of real part of dielectric permittivity against frequency. (c) Plot of dielectric loss against frequency for La_{1-x}Sr_xCoO₃ perovskite oxides at room temperature with 20 Hz – 3 MHz frequency range.

regions, which may cause the dielectric constant to increase. Consequently, the polarization as well as dielectric constant decreases at high frequency and reaches to a constant value because the ions do not have enough time to accumulate at the interface. Fig. 8c shows frequency effect on dielectric loss ($\tan\delta$) at room temperature. It is clear from the results that the loss tangent decreases with increasing frequency, which exhibit dispersion behaviour similar to dielectric constant. Relatively high conducting behaviour at low frequency could be related with polarization changes and charge exchange between cobalt ions. This dielectric behavior of La_{1-x}Sr_xCoO₃ perovskite oxide materials could be attributed to Maxwell-Wagner interfacial polarization model with Koop's phenomenological theory.

4. Conclusion

La_{1-x}Sr_xCoO₃ perovskite oxides (x = 0.0, 0.20, 0.50, 0.80) were successfully synthesized using the sol-gel method. The crystal structure of La_{1-x}Sr_xCoO₃ perovskite oxides was changed from rhombohedral to primitive cubic structure with Sr-doping as also confirmed by Rietveld refinement. Sr-doped dependent electrical properties of La_{1-x}Sr_xCoO₃ perovskite oxides have been improved by Sr-substitution of La. Frequency dependent dielectric properties of La_{1-x}Sr_xCoO₃ perovskite materials were constant at high frequency.

Declaration of Competing Interest

The authors declare that they have no known competing financial interests or personal relationships that could have appeared to influence the work reported in this paper.

Acknowledgement

The authors extend their grateful appreciation to the Deanship of Scientific Research at King Saud University for funding their research group (RG-1435-007). This work was also funded by the Deanship of Scientific Research at Princess Nourah Bint Abdulrahman University through the Fast-track Research Funding Program.

References

- Ahmed, J., Alam, M., Majeed Khan, M.A., Alshehri, S.M., 2021. Bifunctional electrocatalytic performances of NiMoO₄-NRs@RGO nanocomposites for oxygen evolution and oxygen reduction reactions. *J. King Saud Univ. Sci.* 33, 101317. <https://doi.org/10.1016/j.jksus.2020.101317>.
- Ahmed, J., Alhokbany, N., Ubaidullah, M., Mutehri, S., Khan, M.A.M., Alshehri, S.M., 2020. Synthesis of double perovskite La₂MnNiO₆ nanoparticles as highly efficient oxygen evolution electro-catalysts. *Ceram. Int.* 46, 20038–20044. <https://doi.org/10.1016/j.ceramint.2020.05.075>.
- Ahmed, J., Poltavets, V.V., Prakash, J., Alshehri, S.M., Ahamad, T., 2016. Sol-gel synthesis, structural characterization and bifunctional catalytic activity of nanocrystalline delafossite CuGaO₂ particles. *J. Alloys Compounds* 688 (1157–1161). <https://doi.org/10.1016/j.jallcom.2016.07.017>.
- Alhokbany, N.S., Mohammed Qadri, N., Ahmed, J., Ahamad, T., Alshehri, S.M., 2020. Flux synthesis, crystal structure and electrochemical properties of Na₂La₂P₄O₁₂ material for supercapacitors. *Mater. Lett.* 272, 127803. <https://doi.org/10.1016/j.matlet.2020.127803>.
- Bellakki, M.B., Madhu, C., Greindl, T., Kohli, S., McCurdy, P., Manivannan, V., 2010. Synthesis and measurement of structural and magnetic properties of K-doped LaCoO₃ perovskite materials. *Rare Metals* 29, 491–500. <https://doi.org/10.1007/s12598-010-0155-7>.
- Björketun, M.E. et al., 2017. Defect chemistry and electrical conductivity of Sm-doped La_{1-x}Sr_xCoO_{3-δ} for solid oxide fuel cells. *J. Phys. Chem. C* 121, 15017–15027. <https://doi.org/10.1021/acs.jpcc.7b02608>.
- Cheng, X. et al., 2015. Oxygen evolution reaction on La_{1-x}Sr_xCoO₃ perovskites: A combined experimental and theoretical study of their structural electronic, and

- electrochemical properties. *Chem. Mater.* 27, 7662–7672. <https://doi.org/10.1021/acs.chemmater.5b03138>.
- Chennabasappa, M., Petit, E., Toulemonde, O., 2020. Toward oxygen fully stoichiometric $\text{La}_{1-x}\text{Sr}_x\text{CoO}_3$ ($0.5 \leq x \leq 0.9$) perovskites: Itinerant magnetic mechanism more than double exchange one's. *Ceram. Int.* 46, 6067–6072. <https://doi.org/10.1016/j.ceramint.2019.11.067>.
- Dobler, D., Oswald, S., Wetzig, K., 2002. Calibration of XPS – energy scale for determination of the oxidation states of doping elements in SnO_2 powders. *Anal. Bioanal. Chem.* 374, 646–649. <https://doi.org/10.1007/s00216-002-1448-y>.
- Fang, Z. et al., 2016. Optical properties and thermal stability of $\text{La}_{1-x}\text{Sr}_x\text{CoO}_3-\delta$ ($0.2 \leq x \leq 0.8$) ceramics. *Solar Energy* 137, 73–79. <https://doi.org/10.1016/j.solener.2016.07.057>.
- Farhadi, S., Sepahvand, S., 2010. Microwave-assisted solid-state decomposition of $\text{La}[\text{Co}(\text{CN})_6]_5\text{H}_2\text{O}$ precursor: A simple and fast route for the synthesis of single-phase perovskite-type LaCoO_3 nanoparticles. *J. Alloys Compounds* 489 (586–591). <https://doi.org/10.1016/j.jallcom.2009.09.117>.
- Fu, S. et al., 2013. Low temperature synthesis and photocatalytic property of perovskite-type LaCoO_3 hollow spheres. *J. Alloys Compounds* 576 (5–12). <https://doi.org/10.1016/j.jallcom.2013.04.092>.
- Haron, W., Wisitsoraat, A., Wongnawa, S., 2017. Nanostructured perovskite oxides – LaMO_3 (M=Al, Co, Fe) prepared by co-precipitation method and their ethanol-sensing characteristics. *Ceram. Int.* 43, 5032–5040. <https://doi.org/10.1016/j.ceramint.2017.01.013>.
- Huang, K., Lee, H.Y., Goodenough, J.B., 1998. Sr- and Ni-doped LaCoO_3 and LaFeO_3 Perovskites: New cathode materials for solid-oxide fuel. *Cells J. Electrochem. Soc.* 145 (3220–3227). <https://doi.org/10.1149/1.1838789>.
- Hwang, J., Rao, R.R., Giordano, L., Katayama, Y., Yu, Y., Shao-Horn, Y., 2017. Perovskites in catalysis and electrocatalysis. *Science* 358, 751. <https://doi.org/10.1126/science.aam7092>.
- Iwasaki, K., Ito, T., Nagasaki, T., Arita, Y., Yoshino, M., Matsui, T., 2008. Thermoelectric properties of polycrystalline $\text{La}_{1-x}\text{Sr}_x\text{CoO}_3$. *J. Solid State Chem.* 181, 3145–3150. <https://doi.org/10.1016/j.jssc.2008.08.017>.
- Jayapandi, S., Lakshmi, D., Premkumar, S., Packiyaraj, P., Anitha, K., 2018. Augmented photocatalytic and electrochemical activities of Ag tailored LaCoO_3 perovskite semiconductor. *Mater. Lett.* 218, 205–208. <https://doi.org/10.1016/j.matlet.2018.02.015>.
- Khan, S.A. et al., 2018. Crystal-site engineering for developing tunable green light emitting $\text{Ba}_9\text{Lu}_2\text{Si}_6\text{O}_{24}:\text{Eu}^{2+}$ phosphors for efficient white LEDs. *J. Alloys Compounds* 767 (374–381). <https://doi.org/10.1016/j.jallcom.2018.07.107>.
- Khan, S.A. et al., 2017. Single-phase white light-emitting $\text{Ca}_x\text{Ba}(9-x)\text{Lu}_2\text{Si}_6\text{O}_{24}:\text{Eu}^{2+}/\text{Mn}^{2+}$ phosphors. *ACS Omega* 2, 6270–6277. <https://doi.org/10.1021/acsomega.7b00985>.
- Kun, R., Populoh, S., Karvonen, L., Gumbert, J., Weidenkaff, A., Busse, M., 2013. Structural and thermoelectric characterization of Ba substituted LaCoO_3 perovskite-type materials obtained by polymerized gel combustion method. *J. Alloys Compounds* 579 (147–155). <https://doi.org/10.1016/j.jallcom.2013.05.019>.
- Lal, B., Raghunandan, M.K., Gupta, M., Singh, R.N., 2005. Electrocatalytic properties of perovskite-type $\text{La}_{1-x}\text{Sr}_x\text{CoO}_3$ ($0 \leq x \leq 0.4$) obtained by a novel stearic acid sol-gel method for electrocatalysis of O_2 evolution in KOH solutions. *Int. J. Hydrogen Energy* 30 (723–729). <https://doi.org/10.1016/j.ijhydene.2004.07.002>.
- Li, T., Jayathilake, R.S., Taylor, D.D., Rodriguez, E.E., 2019. Structural studies of the perovskite series $\text{La}_{1-x}\text{Sr}_x\text{CoO}_3-\delta$ during chemical looping with methane. *Chem. Commun.* 55, 4929–4932. <https://doi.org/10.1039/C8CC09573F>.
- Liu, B., Wang, Y., Liu, G., Feng, H., Yang, H., Sun, J., 2016. Electrical transport properties of $\text{La}_{1-x}\text{Sr}_x\text{CoO}_3$ thin films. *J. Appl. Phys.* 120 (154103). <https://doi.org/10.1063/1.4964946>.
- Liu, H., Guo, Y., Xie, R., Peng, T., Ma, G., Tang, Y., 2017. Novel acetone sensing performance of $\text{La}_{1-x}\text{Sr}_x\text{CoO}_3$ nanoparticles at room temperature. *Sens. Actuat. B Chem.* 246, 164–168. <https://doi.org/10.1016/j.snb.2017.02.072>.
- Long, P.T., Manh, T.V., Ho, T.A., Dongquoc, V., Zhang, P., Yu, S.C., 2018. Magnetocaloric effect in $\text{La}_{1-x}\text{Sr}_x\text{CoO}_3$ undergoing a second-order phase transition. *Ceram. Int.* 44, 15542–15549. <https://doi.org/10.1016/j.ceramint.2018.05.216>.
- Lu, Y. et al., 2020. Experimental and theoretical study on enhanced electrical properties of nickel-substituted $\text{La}_{0.5}\text{Sr}_{0.5}\text{CoO}_{3-\delta}$ ceramics. *J. Eur. Ceram. Soc.* 40, 3049–3056. <https://doi.org/10.1016/j.jeurceramsoc.2020.02.063>.
- Lu, Y. et al., 2019. Engineering oxygen vacancies into LaCoO_3 perovskite for efficient electrocatalytic oxygen evolution. *ACS Sustain. Chem. Eng.* 7, 2906–2910. <https://doi.org/10.1021/acssuschemeng.8b05717>.
- Mefford, J.T. et al., 2016. Water electrolysis on $\text{La}_{1-x}\text{Sr}_x\text{CoO}_3-\delta$ perovskite electrocatalysts. *Nat. Commun.* 7, 11053. <https://doi.org/10.1038/ncomms11053>.
- Mineshige, A., Inaba, M., Yao, T., Ogumi, Z., Kikuchi, K., Kawase, M., 1996. Crystal structure and metal-insulator transition of $\text{La}_{1-x}\text{Sr}_x\text{CoO}_3$. *J. Solid State Chem.* 121 (423–429). <https://doi.org/10.1006/jssc.1996.0058>.
- Nakayama, S., Okazaki, M., Aung, Y.L., Sakamoto, M., 2003. Preparations of perovskite-type oxides LaCoO_3 from three different methods and their evaluation by homogeneity, sinterability and conductivity. *Solid State Ion.* 158, 133–139. [https://doi.org/10.1016/S0167-2738\(02\)00767-1](https://doi.org/10.1016/S0167-2738(02)00767-1).
- Petrov, A.N., Kononchuk, O.F., Andreev, A.V., Cherepanov, V.A., Kofstad, P., 1995. Crystal structure, electrical and magnetic properties of $\text{La}_{1-x}\text{Sr}_x\text{CoO}_3-y$. *Solid State Ion.* 80, 189–199. [https://doi.org/10.1016/0167-2738\(95\)00114-L](https://doi.org/10.1016/0167-2738(95)00114-L).
- Rehman, S.U., Song, R.-H., Lim, T.-H., Park, S.-J., Hong, J.-E., Lee, J.-W., Lee, S.-B., 2018. High-performance nanofibrous LaCoO_3 perovskite cathode for solid oxide fuel cells fabricated via chemically assisted electrodeposition. *J. Mater. Chem. A* 6 (16), 6987–6996. <https://doi.org/10.1039/C7TA10701C>.
- Reis, M.S. et al., 2017. Spin state and magnetic ordering of half-doped $\text{Nd}_{0.5}\text{Sr}_{0.5}\text{CoO}_3$ cobaltite. *J. Magn. Magn. Mater.* 422 (197–203). <https://doi.org/10.1016/j.jmmm.2016.08.080>.
- Rodriguez-Carvajal, J., 1993. Recent advances in magnetic structure determination by neutron powder diffraction. *Phys. B Condensed Matter* 192 (1–2), 55–69. [https://doi.org/10.1016/0921-4526\(93\)90108-1](https://doi.org/10.1016/0921-4526(93)90108-1).
- Viskadorakis, Z., Athanasopoulos, G.I., Kasotakis, E., Giapintzakis, J., 2016. Effect of microstructure on the thermoelectric performance of $\text{La}_{1-x}\text{Sr}_x\text{CoO}_3$. *J. Solid State Chem.* 243, 111–118. <https://doi.org/10.1016/j.jssc.2016.08.015>.
- Viskadorakis, Z., Pervolaraki, M., Athanasopoulos, G.I., Giapintzakis, J., 2019. Thermoelectric properties of strained, lightly-doped $\text{La}_{1-x}\text{Sr}_x\text{CoO}_3$ thin films. *J. Appl. Phys.* 125 (055102). <https://doi.org/10.1063/1.5054734>.
- Wang, K., Song, J., Duan, X., Mu, J., Wang, Y., 2017. Perovskite LaCoO_3 nanoparticles as enzyme mimetics: Their catalytic properties, mechanism and application in dopamine biosensing. *New J. Chem.* 41 (16), 8554–8560. <https://doi.org/10.1039/C7NJ01177F>.
- Wang, Y., Sui, Y., Wang, X., Su, W., Cao, W., Liu, X., 2010. Thermoelectric response driven by spin-state transition in $\text{La}_{1-x}\text{Ce}_x\text{CoO}_3$ perovskites. *ACS Applied Materials & Interfaces* 2, 2213–2217. <https://doi.org/10.1021/am100243e>.
- Wu, Y.-C., Huang, P.-Y., Xu, G., 2017. Properties and microstructural analysis of $\text{La}_{1-x}\text{Sr}_x\text{CoO}_3-\delta$ ($x=0-0.6$) cathode materials. *Ceram. Int.* 43, 2460–2470. <https://doi.org/10.1016/j.ceramint.2016.11.041>.
- Zhu, Z., Shi, Y., Aruta, C., Yang, N., 2018. Improving electronic conductivity and oxygen reduction activity in Sr-doped lanthanum cobaltite thin films: Cobalt valence state and electronic band structure effects. *ACS Appl. Energy Mater.* 1, 5308–5317. <https://doi.org/10.1021/acsaem.8b00931>.